Inorg. Chem. **2008**, *47*, 10330−10341

Ni(II) and *hs*-Fe(II) Complexes of a Paramagnetic Thiazyl Ligand, and Decomposition Products of the Iron Complex, Including an Fe(III) Tetramer

Nigel G. R. Hearns,[†] Elisabeth M. Fatila,[†] Rodolphe Clérac,[‡] Michael Jennings,[§] and Kathryn E. Preuss*,[†]

Department of Chemistry, University of Guelph, 50 Stone Road East, Guelph, Ontario N1G 2W1, Canada, Université Bordeaux 1, CNRS - Centre de Recherche Paul Pascal (CRPP) UPR 8641, 115 avenue du Dr. A. Schweitzer, 33600 Pessac, France, and Department of Chemistry, University of Western Ontario, London, Ontario N6A 5B7, Canada

Received April 28, 2008

Synthesis and structural, magnetic and electrochemical characterization of the Ni(hfac)$_2$(pyDTDA) and the Fe(hfac)$_2$(pyDTDA) complexes are reported (hfac = 1,1,1,5,5,5-hexafluoroacetylacetonato-; pyDTDA = 4-(2′-pyridyl)-1,2,3,5-dithiadiazolyl). Unlike the previously reported Mn(II) and Cu(II) complexes, but similar to the Co(II) complex, the Ni(II) and Fe(II) complexes are not dimerized in the solid state, allowing for magnetic coupling between the metal ion and paramagnetic ligand to be readily obtained from solid state magnetic measurements: Ni complex, $J/k_B = +132(1)$ K, using $\boldsymbol{H} = -2J\{\boldsymbol{S}_{Ni} \cdot \boldsymbol{S}_{Rad}\}$ and $g_{Ni} = 2.04(2)$ and $g_{Rad} = 1.99(2)$; Fe complex, $J/k_B = -60.3(3)$ K, using $\boldsymbol{H} = -2J\{\boldsymbol{S}_{Fe} \cdot \boldsymbol{S}_{Rad}\}$ and $g_{av} = 2.11(2)$. The iron complex is unusually unstable. A thermal decomposition product is isolated wherein the coordinated pyDTDA ligand appears to have been transformed into a coordinated 2-(2′-pyridyl)-4,6-bis(trifluoromethyl)pyrimidine. The iron complex also yields a solution decomposition product in the presence of air that is best described as an oxygen bridged iron(III) tetramer with two hfac ligands on each of three iron atoms and two oxidized pyDTDA ligands chelated on the fourth.

Introduction

The development of molecule based magnetic materials is currently a topic of significant interest.[1] One of the possible approaches toward this goal involves the use of paramagnetic ligands. When coordinated to paramagnetic metal ions, these ligands can increase the overall magnetic spin of the complex and can be used to mediate magnetic coupling between paramagnetic metal centers by providing direct exchange coupling pathways.[2] Some classes of paramagnetic ligand, such as nitroxide based radicals[3] and semiquinones,[4] have enjoyed extensive study. Others, such as thiazyl based radicals,[5] remain largely overlooked.

Reporting the Ni(II) and high spin Fe(II) complexes of pyDTDA (complexes **1** and **2** respectively), we herein complete a series of first row transition metal dication complexes of this paramagnetic thiazyl ligand (Chart 1). This concludes the first comprehensive study of multiple coordination complexes of a thiazyl based spin-bearing ligand. We find a trend in the nature of the exchange coupling between the pyDTDA ligand and the metal ion that can be explained using a simple magnetic orbital overlap model. We also find a trend in the propensity for π-stacked dimer

* To whom correspondence should be addressed. E-mail: kpreuss@uoguelph.ca.
† University of Guelph.
‡ Université Bordeaux 1, CNRS - CRPP.
§ University of Western Ontario.

(1) (a) Deumal, M.; Robb, M. A.; Novoa, J. J. In *Topics in the Theory of Chemical and Physical Systems*; Lahmar, S. et al., Eds.; Springer: New York, 2007; pp 271−289. (b) Miller, J. S. *MRS Bulletin* **2007**, *32*, 549. (c) Bogani, L.; Wernsdorfer, W. *Nat. Mater.* **2008**, *7*, 179.
(2) Kahn, O. *Molecular Magnetism*; Wiley-VCH: New York, 1993.
(3) (a) Osanai, K.; Okazawa, A.; Nogami, T.; Ishida, T. *J. Am. Chem. Soc.* **2006**, *128*, 14008. (b) Osiecki, J. H.; Ullman, E. F. *J. Am. Chem. Soc.* **1972**, *94*, 7049. (c) Luneau, D.; Risoan, G.; Rey, P.; Grand, A.; Caneschi, A.; Gatteschi, D.; Laugier, J. *Inorg. Chem.* **1993**, *32*, 5616. (d) Kaizaki, S. *Coord. Chem. Rev.* **2006**, *250*, 1804.
(4) (a) ShultzD. A. In *Magnetism: Molecules to Materials II: Molecule-based Materials*, Miller, J. S., Drillon, M., Eds.; Wiley-VCH: New York, 2001; pp 281−306. (b) Hendrickson, D. N.; Pierpont, C. G. *Top. Curr. Chem.* **2004**, 234–63. (c) Pierpont, C. G. *Coord. Chem. Rev.* **2001**, *216*, 99.
(5) (a) Preuss, K. E. *Dalton Trans.* **2007**, 2357. (b) Rawson, J. M.; Alberola, A.; Whalley, A. *J. Mater. Chem.* **2006**, *16*, 2560. (c) Awaga, K.; Tanaka, T.; Shirai, T.; Fujimori, M.; Suzuki, Y.; Yoshikawa, H.; Fujita, W. *Bull. Chem. Soc. Jpn.* **2006**, *79*, 25.

10.1021/ic800749b CCC: $40.75
Published on Web 10/17/2008

Chart 1

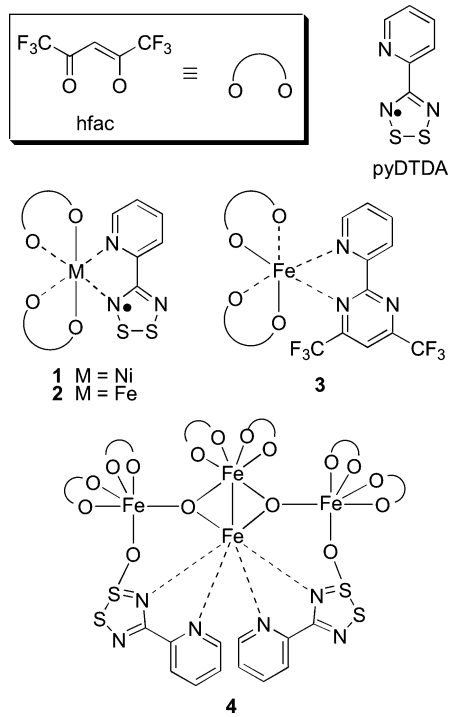

Chart 2

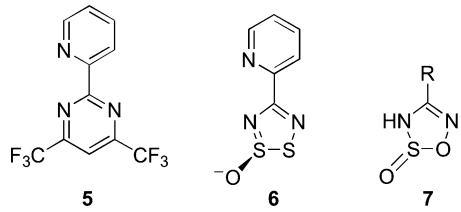

formation that is related to the local coordination geometry of the metal ion.

In addition, we report an unusual decomposition product **3** and an oxidation product **4** of the iron complex **2**, both of which have been identified by single crystal X-ray structural analysis. A thermal decomposition product **3** can be reproducibly recovered by heating **2** under a weak static vacuum. Complex **3** is composed of an $Fe(hfac)_2$ fragment chelated by a previously unknown ligand, 2-(2′-pyridyl)-4,6-bis(trifluoromethyl)pyrimidine **5** (Chart 2). The structure of this complex suggests a decomposition pathway involving at least two molecules of **2**; however, the mechanism and other byproducts have not been identified. The air-exposed solution decomposition product **4** is an oxygen bridged Fe(III) tetramer. Interestingly, a major rearrangement of complex **2** must occur such that two pyDTDA ligands end up coordinated to a common iron ion. Upon inspection, a close contact between an iron-bound oxygen atom and one of the pyDTDA sulfur atoms is found. Thus, the pyDTDA ligand is not paramagnetic in complex **4** and is best regarded as the novel 1,2,3,5-dithiadiazolyl-1-oxide anion **6**.

Experimental Section

General Considerations. Reactions and manipulations were performed under argon atmosphere unless otherwise stated. Organic solvents were dried and distilled under argon prior to use: THF dried over Na/benzophenone, and CH_2Cl_2 and 1,2-dichloroethane dried over CaH_2. Reagents were purchased from Aldrich and used as received. The pyDTDA ligand was prepared following literature procedure.[6] The $M(hfac)_2 \cdot 2H_2O$ (M = Ni, Fe) starting material was prepared following a literature procedure[7] and converted to the tetrahydrofuran adduct, $M(hfac)_2 \cdot 2THF$, by recrystallization from dry THF; the absence of an O−H stretching band at about 3410 cm^{-1} in the IR (KBr pressed pellet) indicates the absence of coordinated water. The $Fe(hfac)_2 \cdot 2THF$ was sublimed under dynamic vacuum (10^{-2} torr, 50 °C) prior to cyclic voltammetry measurements. IR spectra were obtained on a Nicolet 510-FTIR spectrometer at ambient temperature. ^1H NMR spectra were recorded on a Brüker Avance 400 MHz spectrometer. Mass spectra were collected by the University of Waterloo Mass Spectrometry Facility, Waterloo, ON, Canada, using a JEOL HX110 double focusing mass spectrometer. Elemental analyses were performed by MHW Laboratories in Phoenix, AZ.

$Ni(hfac)_2$(pyDTDA) 1. Dry CH_2Cl_2 (7 mL) was added to a solid mixture of $Ni(hfac)_2 \cdot 2THF$ (0.4120 g, 0.6677 mmol) and pyDTDA (0.1225 g, 0.6722 mmol) under an inert atmosphere. The resulting dark red solution was stirred for 0.5 h at ambient temperature. The solvent was removed in vacuo to afford an amorphous purple solid. This crude product was sublimed at 120 °C under dynamic vacuum (10^{-3} torr) over 18 h generating **1** as pure, microcrystalline material; yield 0.3773 g (0.5760 mmol, 86%). Shiny brown blocks of **1** suitable for X-ray crystallography were grown by slow sublimation over 4 weeks at 125 °C under static vacuum (10^{-2} torr). IR (KBr): 3286, 3142, 3103, 1650, 1637, 1605, 1555, 1527, 1486, 1403, 1349, 1319, 1255, 1194, 1145, 1098, 1049, 1025, 950, 923, 870, 812, 792, 762, 51, 743, 671, 650, 587, 529, 485, 421 cm^{-1}. Mass spec. (CI NH_3(g), 5 × 10^{-6} torr, 200 eV, 200 °C): *m/z* 672 ($M^+ + NH_4$) 10%, 629 ($M^+ - 43$), 464 ($[M^+ + NH_4] - C_5HO_2F_6$), 447 ($M^+ - C_5HO_2F_6$) 100%, 386, 183 ($C_6H_4N_3S_2$ + H). Anal. Calcd. for $NiC_{16}H_6N_3S_2O_4F_{12}$: C, 29.34; H, 0.92; N, 6.41%. Found: C, 29.57; H, 0.84; N, 6.60%.

$Fe(hfac)_2$(pyDTDA) 2. pyDTDA (0.6383 g, 3.502 mmol) was dissolved in 10 mL of anhydrous CH_2Cl_2 under inert atmosphere and transferred into a solution of $Fe(hfac)_2 \cdot 2THF$ (2.1515 g, 3.503 mmol) dissolved in 10 mL of anhydrous CH_2Cl_2. The resulting dark purple solution was stirred for 0.5 h at 30 °C. The solvent was removed in vacuo to afford a dark red solid that was purified by static vacuum sublimation (10^{-3} torr) at 100 °C overnight affording **2** as dark purple blocks; yield 1.753 g (2.688 mmol, 77%). IR(KBr): 3141(w), 3103(w), 3084(w), 1634 (s), 1601(s), 1555(s), 1526(s), 1477(s), 1452(s), 1401(s), 1348(m), 1315(w), 1256(vs), 1192(vs), 1147(vs), 1097(s), 1049(m), 1019(m), 950(m), 856(m), 809(m), 793(s), 762(w), 750(w), 743(m), 665(s), 793(s), 665(s), 652(m), 641(w), 587(m), 524(m), and 414(w) cm^{-1}. Anal. Calcd. for $FeC_{16}H_6N_3S_2O_4F_{12}$: C, 29.46; H, 0.92; N, 6.44%. Found: C, 29.54; H, 0.85; N, 6.23%.

$Fe(hfac)_2$(2-(2′-pyridyl)-4,6-bis(trifluoromethyl)pyrimidine) 3. Crude, dark red solid **2** was heated in a glass tube sealed under static vacuum (10^{-1} torr) at temperatures ranging from 50 to 100 °C overnight. Red needle-like crystals of **3** were recovered from the room temperature region of the glass tube. The yield was not determined. IR (KBr): 3148 (w), 1618 (s), 1570 (m), 1543 (m), 1437 (m), 1420 (m), 1252 (s), 1212 (s), 1145 (s), 1108 (m), 818 (m), 746 (m), 665 (m), 593 (m), 516 (w) cm^{-1}. Mass spec. (CI

(6) Hearns, N. G. R.; Preuss, K. E.; Richardson, J. F.; Bin-Salamon, S. *J. Am. Chem. Soc.* **2004**, *126*, 9942.
(7) (a) Preuss, K. E.; Wu, J.; Jennings, M. *Acta Crystallogr.* **2005**, *E61*, m430. (b) Journaux, Y.; Kahn, O.; Morgenstern-Badarau, I.; Galy, J.; Jaud, J.; Bencini, A.; Gatteschi, D. *J. Am. Chem. Soc.* **1985**, *107*, 6305.

NH_3(g), 5×10^{-6} torr, 200 eV, 200 °C): *m/z* 762.9 (M^+, 2%), 294 ($C_{11}H_5N_3F_6^+$, 100%).

$Fe_4O_2(hfac)_6$(1,2,3,5-dithiadiazolyl-1-oxide)$_2$ 4. Pure, crystalline **2** was dissolved in hot chlorobenzene under ambient atmosphere. This solution was allowed to sit, undisturbed, exposed to the air for 5 days. Dark red plate-like crystals were recovered. The yield was not determined, and **4** was identified by single crystal X-ray diffraction alone.

Reaction of pyDTDA and 1,1,1,5,5,5-Hexafluoro-2,4-pentanedione (Hhfac). pyDTDA (0.4246 g, 2.317 mmol) was dissolved in 24 mL of dry 1,2-dichloroethane under argon. Hhfac (0.35 mL, 2.507 mmol) was syringed into the solution. After 1 h of stirring under argon at 40 °C, no color change was observed and no precipitate had formed. The solvent was removed in vacuo, and the resulting brown residue was submitted to sublimation conditions under dynamic vacuum (10^{-2} torr, 100 °C). Yellow crystals of elemental sulfur were recovered from the sublimation. The remaining non-volatile brown powder was analyzed by TLC (CH_2Cl_2 and 1% triethylamine) and determined to be composed of at least four components that could be eluted from the baseline, two colorless and two yellow. These were separated on a short silica column, using 500 mL of CH_2Cl_2 (1% triethylamine) as eluent. The four mobile components were analyzed by ^{1}H NMR, and it was determined that the residue contained three components with peaks in the aromatic region. The integration and coupling pattern of the peaks confirm that **5** was not a product of this reaction. Two of the components also showed a singlet in the aromatic region; however, the highly solvent dependent nature of this singlet peak, the integration, and downfield chemical shift of over 9 ppm in DMSO all support the conclusion that the isolated compounds are not ligand **5**.

Reaction of pyDTDA and [Na(benzo-15-crown-5)][hfac]. NaH (0.6 g, 30 mmol) was suspended in 20 mL of dry CH_2Cl_2. Hhfac (2.4 mL, 17 mmol) was added dropwise, stirring under argon. The evolution of gas and formation of a white precipitate was observed. After 24 h, the CH_2Cl_2 was removed in vacuo, and the remaining white solid Na(hfac) was analyzed by FT-IR (nujol mull): 1671.7 (s), 1611.7 (w), 1556.4 (m), 1531.1 (s), 1486.9 (s), 1463.1 (s), 1376.6 (m), 1338.4 (mw), 1258.2 (s), 1206.9 (s), 1132.6 (s), 801.8 (m), 739.6 (w), 722.2 (w), 664.4 (m), 580.7 (mw) cm^{-1}.

[Na(benzo-15-crown-5)][hfac] was prepared by reacting a suspension of Na(hfac) with benzo-15-crown-5-ether. IR (KBr): 2936.5 (m), 2915.0 (m), 2874.2 (m), 1675.4 (s), 1598.1 (mw), 1550.8 (m), 1532.0 (m), 1505.6 (m), 1472.6 (mw), 1460.4 (m), 1362.0 (w), 1349.6 (w), 1322.8 (w), 1255.0 (s), 1211.2 (m), 1191.5 (m), 1170.9 (m), 1123.5 (s), 1101.3 (m), 1061.7 (w), 1047.4 (m), 954.9 (m), 942.8 (m), 919.4 (w), 857.3 (w), 833.0 (w), 788.7 (mw), 778.0 (w), 755.7 (m), 658.9 (m), 604.9 (w), 575.1 (m) cm^{-1}.^{1}H NMR (DMSO): 3.6049 (m, 8H), 3.7551 (m, 4H), 4.0254 (m, 4H), 5.3055 (s, 1H), 6.8704 (m, 2H), 6.9352 (m, 2H) ppm.

For the purpose of reaction with pyDTDA, the following procedure was used: Na(hfac) (0.3205 g, 1.393 mmol) was suspended in 20 mL of CH_2Cl_2. Under argon, benzo-15-crown-5-ether (0.3682 g, 1.372 mmol) was added, and the white suspension became a clear solution after 20 min. After 24 h of stirring under argon, the solution was transferred via syringe to a solution containing excess pyDTDA (0.2715 g, 1.490 mmol) in 10 mL of CH_2Cl_2. The resulting purple-red solution was allowed to stir under argon for 1 h. No precipitate was observed, so the CH_2Cl_2 solvent was removed in vacuo, and the purple-black solid residue was submitted to sublimation conditions under dynamic vacuum (10^{-2} torr, 100 °C). Purple-black crystals of pyDTDA (confirmed by FT-IR) were sublimed. FT-IR and ^{1}H NMR analyses of the remaining unsublimed light gray powder confirmed that there was no reaction between pyDTDA and [Na(benzo-15-crown-5-ether][hfac]. IR (KBr): 2944.2 (m), 2879.5 (m), 1670.9 (s), 1599.1 (m), 1548.7 (m), 1533.3 (ms), 1505.3 (m), 1475.4 (m), 1457.9 (m), 1362.6 (m), 1346.9 (mw), 1328.5 (mw), 1253.8 (s), 1213.7 (ms), 1194.1 (ms), 1122.5 (s), 1103.4 (s), 1062.3 (m), 1047.9 (ms), 954.2 (m), 943.0 (m), 787.8 (m), 751.4 (ms), 659.2 (ms), 574.8 (m) cm^{-1}. ^{1}H NMR (DMSO): 3.6109 (m, 8H), 3.7627 (m, 4H), 4.0439 (m, 4H), 5.3866 (s, 1H), 6.8704 (m, 2H), 6.9352 (m, 2H) ppm. Weaker signals were observed in the aromatic region; however, no singlet peak was observed upfield of 10.3 ppm.

Magnetometry. Magnetic susceptibility measurements were obtained using a Quantum Design SQUID magnetometer MPMS-XL with a working temperature of 1.8 to 400 K for direct current (dc) applied fields from −7 to 7 T. Polycrystalline samples (22.4 mg) of **1** and (42.5 mg) **2**, generated by sublimation and pure by elemental analysis, were used for magnetometry measurements. The samples were handled under argon atmosphere and sealed in a plastic bag to avoid any contact with air or water. The magnetic data were corrected for the sample holder and the diamagnetic contribution. The absence of ferromagnetic impurities was verified by checking the linear applied-field dependence of the magnetization from 0 to 70,000 Oe, at 100 K.

Cyclic Voltammetry. Electrochemical measurements were performed at ambient temperature, using an Autolab PGSTAT 30 instrument. Analyte solutions (ca. 2 mM) were prepared in anhydrous, degassed CH_2Cl_2, with 0.05 M nBu$_4$NPF$_6$ as supporting electrolyte. A three-electrode glass cell, sealed under argon atmosphere, was employed; Pt wire electrodes (working, reference, and counter). Electrodes were decontaminated using a hydrogen flame prior to use. The ferrocene/ferrocenium couple ($E_{1/2} = 0.48$ V vs SCE under these conditions)[8] was used as an internal reference. All data are reported versus SCE. Multiple applied scan rates ranging from 0.05 to 1.00 $V \cdot s^{-1}$ were employed to measure the cyclic voltammetric response of **1** and **2**. From plots of the square root of scan rate versus maximum peak current of major peaks in both samples, it was determined that an applied scan rate of 0.5 $V \cdot s^{-1}$ provides representative data (i.e., the square root of this scan rate is in the linear regime when plotted against peak currents of all major processes ensuring that all electron transfer processes are diffusion-controlled rather than surface-controlled);[9] thus, all data reported herein have been obtained at this scan rate (see Supporting Information for scan rate dependent data).

Crystallographic Measurements. Crystals of **1**, **2**, and **4** were prepared at the University of Guelph and delivered to the University of Western Ontario where a representative crystal was mounted on a goniometer head for structural determination by single crystal X-ray diffraction. Data were collected at low temperature (−173 °C) on a Nonius Kappa-CCD area detector diffractometer with COLLECT (Nonius B.V., 1997−2002). Crystals of **3** were prepared at the University of Guelph and delivered to McMaster University where a representative crystal was selected and mounted. Data were collected at ambient temperature on a Bruker APEXII CCD area-detector diffractometer. The unit cell parameters were calculated and refined from the full data set. Crystal cell refinement and data reduction were carried out using HKL2000 DENZO-SMN.[10] Absorption corrections were applied using HKL2000 DENZO-SMN

(8) Boeré, R. T.; Roemmele, T. L. *Coord. Chem. Rev.* **2000**, *210*, 369.
(9) Ji, X.; Chevallier, F. G.; Clegg, A. D.; Buzzeo, M. C.; Compton, R. G. *J. Electroanal. Chem.* **2005**, *581*, 249.
(10) Otwinowski, Z.; Minor, W. *Methods Enzym.* **1997**, *276*, 307.

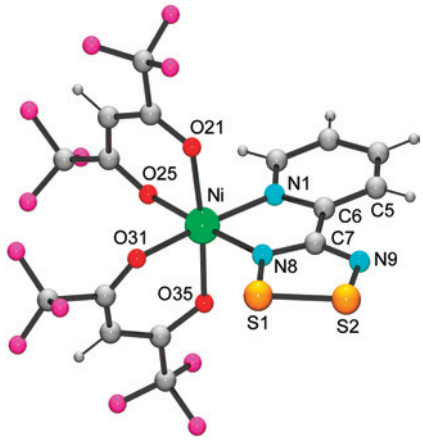

Figure 1. Crystal structure of the Ni(II) complex **1**.

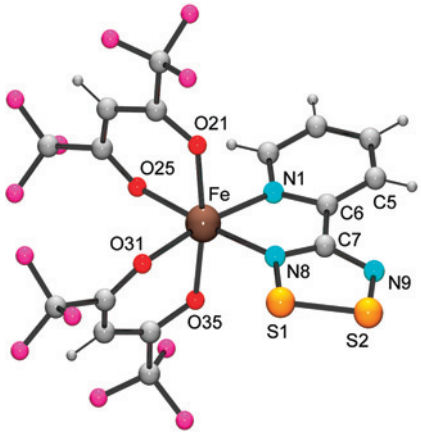

Figure 2. Crystal structure of the Fe(II) complex **2**.

(SCALEPACK). The SHELXTL/PC V6.14 for Windows NT suite of programs[11] was used to solve the structures using direct methods.

Refinement was carried out using the SHELXTL suite of programs and revealed the presence of disorder during the refinement process for both complexes **1** and **2**. These two isostructural complexes both showed disorder involving the pyDTDA ligand, and the same procedure was used to model each. The bidentate ligand has two possible orientations and was modeled as two parts in the refinement. The two parts of the disorder were restrained to be identical. The individual occupancies for the two parts were constrained to total unity but allowed to refine, finally settling in at 0.627/0.373 for **1** and 0.636/0.364 for **2**. The authors felt this allowed the model as much freedom as possible while maintaining a chemically sensible solution.

Results

The Ni(II) complex **1** and the Fe(II) complex **2** are isostructural. The single crystal X-ray structures of these two complexes (Figures 1 and 2, respectively) reveal the chelation of the metal ion by the pyDTDA ligand via two nitrogen atoms, and a pseudo-octahedral coordination geometry about the metal center with bidentate chelation of two hfac ligands completing the coordination sphere. The crystallographic data for both compounds show a disorder that is typical of planar, bidentate ligands such as pyDTDA. The pyDTDA ligand has two possible orientations if the ligand remains planar, and the metal ion coordination geometry remains pseudo-octahedral, yielding two isomers. These two isomers are related by reversing the coordination positions of N1 and N8 with respect to the hfac ligands. One could imagine "flipping" the pyDTDA ligand about an axis perpendicular to the C6−C7 bond and intersecting the metal center. This disorder is shown in Figure 3.

In both complexes, the bond distance to the pyridyl nitrogen atom N1 is slightly shorter than that of the metal ion to the dithiadiazolyl nitrogen atom N8 (see Table 1). In the case of the nickel complex, the M−O bond distances to the two oxygen atoms that are in the same plane as the pyDTDA ligand are roughly equivalent and are shorter than the M−O bond distances to the oxygen atoms in the pseudo-axial positions. The opposite is true in the case of the iron complex.

The two heterocyclic rings of the pyDTDA ligand are roughly coplanar in the coordinated species **1** and are slightly twisted with respect to one another in species **2**. The S1−S2 bond distance in both species is comparable to the intramolecular sulfur−sulfur bond distance in other known 1,2,3,5-dithiadiazolyl neutral radical species.[6] Since the singly occupied molecular orbital (SOMO) of the pyDTDA free radical ligand is π^* in nature, with significant positive spin density at the sulfur atoms, the sulfur−sulfur bond distance may be used as a fair indication of the oxidation state of this species. A shortening of this distance is observed upon one-electron oxidation to the closed shell cation,[12] and a lengthening is expected upon reduction. Little change is observed in the bond length upon coordination to either metal ion; thus, the crystallographic data suggest that the ligand maintains its neutral oxidation state in both complexes.

The crystalline state molecular packing reveals the same regular array of slipped π-stacked coordinated pyDTDA ligands for both complexes **1** and **2** (Figure 3). Being mindful of the disorder described above, there are two possible ways in which the coordinated pyDTDA ligands may be related to one another in terms of crystal packing. The shortest possible *inter*molecular sulfur−sulfur contacts occur between neighboring molecules in the stacking direction of like isomers (Figure 4). The shortest of these in complex **1** is the S2···S2* contact (4.459 Å), which is longer than the shortest intermolecular sulfur−sulfur contact observed in complex **2**; S2···S1* = 4.357 Å (Table 1). The deviation from planarity of the pyDTDA ligand in complex **2** accounts for the shortened contact between S2 and S1*. In both complexes, all sulfur−sulfur contacts are significantly larger than the sum of van der Waals radii for two sulfur atoms (3.6 Å). Thus, the crystal packing indicates the absence of dimer formation between neighboring 1,2,3,5-dithiadiazolyl moieties and suggests that the pyDTDA ligands maintain their radical nature in the solid state.

The magnetic susceptibility of **1** was measured as a function of temperature, from 300 to 1.81 K, at an applied dc field of 1000 Oe. The χT product is plotted as a function of temperature (Figure 5).

At room temperature, the χT product is 1.73 cm^3 K mol^{-1}. Decreasing the temperature, the χT product increases con-

(11) Sheldrick, G. M. *Acta Crystallogr.* **2008**, *A64*, 112.

(12) Ruangsuttinarupap, S.; Gross, H.-D.; Willing, W.; Müller, U.; Dehnicke, K. *Z. Anorg. Allg. Chem.* **1986**, *536*, 153.

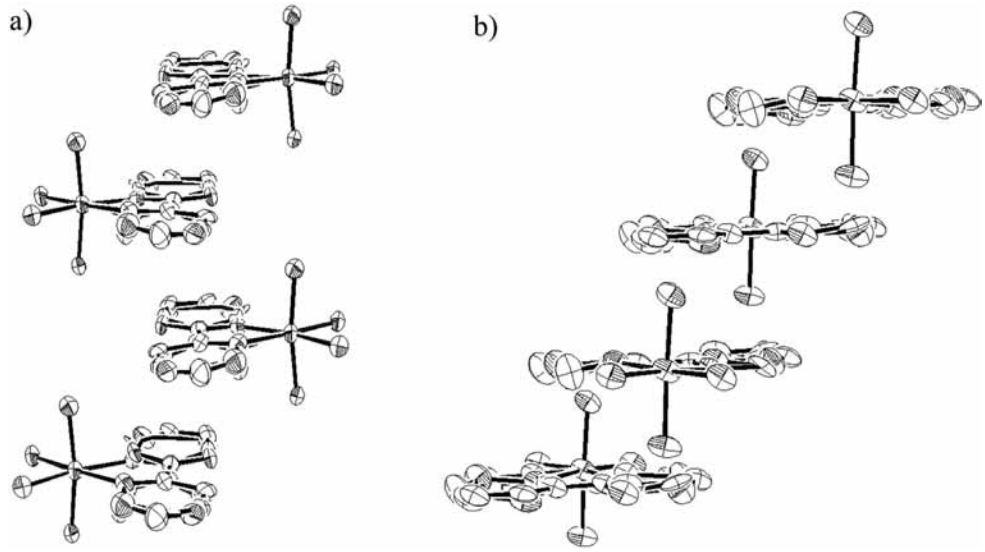

Figure 3. Oak Ridge Thermal Ellipsoid Plot (ORTEP) representation of the Fe(II) complex **2** showing the disorder and the π-stacking as viewed (a) roughly normal to the (101) plane and (b) normal to the (010) plane. Only the oxygen atoms of the hfac ligands are shown, and the hydrogen atoms have been removed for clarity.

Table 1. Summary of Crystallographic Data for **1** and **2**, Including Select Bond Lengths, Contacts, and Torsion Angles

complex	**1**	**2**
molecular formula	$C_{16}H_6F_{12}N_3NiO_4S_2$	$C_{16}H_6F_{12}FeN_3O_4S_2$
molecular weight (g mol^{-1})	655.07	652.21
space group	$Pna2_1$	$Pna2_1$
cell lengths (Å): *a*, *b*, *c*	8.7938(9), 16.3657(10), 15.5980(16)	8.8809(6), 16.6466(9), 15.3774(12)
cell formula units *Z*	4	4
temperature (K)	100(2)	100(2)
bond distance (Å):		
N1−M	2.023(12)	2.126(12)
N8−M	2.082(15)	2.158(14)
bond distance (Å):		
O21−M	2.047(6)	2.055(6)
O25−M	2.018(6)	2.086(6)
O31−M	2.017(6)	2.077(6)
O35−M	2.025(7)	2.059(6)
bond distance (Å):		
S1−S2	2.094(7)	2.077(7)
torsion angle (deg):		
C5−C6−C7−N9	−7(4)	−19(3)
*inter*molecular S−S contacts (Å):		
S1···S2*	4.733	4.873
S2···S1*	4.466	4.357
S2···S2*	4.459	4.513

tinuously to a maximum value of 1.93 cm^3 K mol^{-1} at 70 K, indicating dominant ferromagnetic interactions between

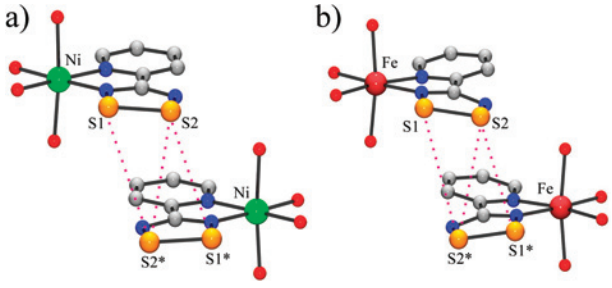

Figure 4. Shortest *inter*molecular sulfur−sulfur contacts (dotted lines) occur between like isomers in the π-stacking direction of both (a) complex **1** and (b) complex **2**.

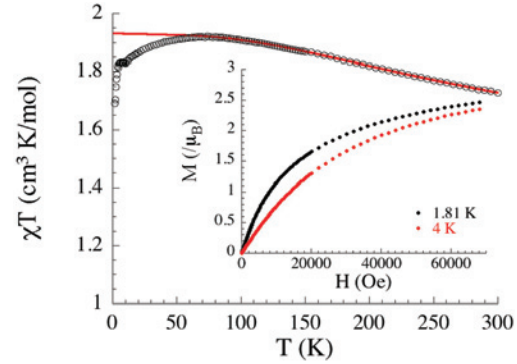

Figure 5. Plot of χT versus T at an applied field of 1000 Oe for complex **1**. The open circles represent measured data points, and the red line indicates the best fit from 300 to 60 K. Inset: plot of M versus H at 1.81 and 4 K.

Ni(II) and the pyDTDA radical ligand. Upon further cooling to 4 K, a gradual decrease in the χT product is observed, followed by a sharp drop in the value of χT below 4 K to a minimum of 1.65 cm^3 K mol^{-1} at 1.81 K. This low temperature behavior is likely the result of weak antiferromagnetic interactions between complexes and, below 4 K, the presence of magnetic anisotropy (zero-field splitting effect).

On the basis of the structure, complex **1** can be viewed as a spin dimer composed of an $S = 1$ Ni(II) ion and an $S = {}^1/_2$ pyDTDA radical ligand. Thus, the magnetic data can be modeled on the basis of an isotropic spin Heisenberg Hamiltonian:

$$\hat{H} = -2J\{\hat{S}_{Ni} \cdot \hat{S}_{Rad}\}$$

where J is a measure of the magnetic coupling interaction between the Ni(II) ion and the pyDTDA radical spins and $\hat{S}_i$ indicates the spin operator for the Ni(II) ion ($S_{Ni} = 1$) and the pyDTDA radical ($S_{Rad} = {}^1/_2$). Applying the van Vleck

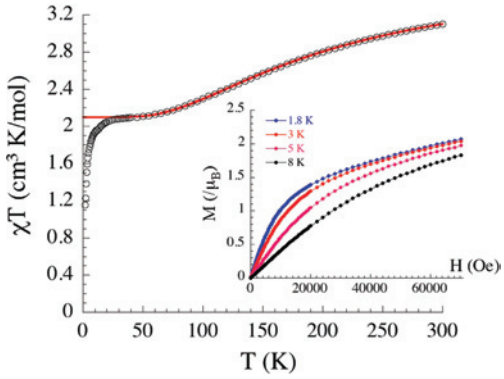

Figure 6. Plot of χT versus T at an applied field of 10,000 Oe for complex **2**. The open circles represent measured data points, and the red line indicates the best fit from 300 to 24 K. Inset: plot of M versus H between 1.81 and 8 K.

equation[13] in the weak field approximation, a theoretical expression for the magnetic susceptibility can be derived:

$$\chi = \frac{N_A \mu_B^2}{4k_B T} \frac{g_{1/2}^2 + 10 g_{3/2}^2 \exp(^{3J}/_{k_B T})}{1 + 2\exp(^{3J}/_{k_B T})}$$

where $g_{1/2} = (4g_{Ni} - g_{Rad})/3$ and $g_{3/2} = (2g_{Ni} + g_{Rad})/3$. The experimental data have been fitted down to 60 K to avoid intermolecular antiferromagnetic interactions or magnetic anisotropy effects. The best set of fitting parameters obtained using this model is $J/k_B = +132(1)$ K, $g_{Ni} = 2.04(2)$, and $g_{Rad} = 1.99(2)$. Defining the spin Hamiltonian as above, the sign of the magnetic interaction implies that this complex possesses an $S_T = {}^3/_2$ spin ground state, thus ferromagnetic coupling between the two unpaired electrons of the d^8 Ni(II) ion and the one unpaired electron of the radical pyDTDA ligand.

The magnetization versus applied magnetic field (M vs H) of **1** was measured from 0 to 70,000 Oe at 1.81 K and at 4 K (Inset, Figure 5). The magnetization at these temperatures does not fully saturate at the maximum applied field, even at 1.81 K (reaching 2.5 μ_B under 7 T), suggesting the presence of significant magnetic anisotropy. Nevertheless, the magnetization appears to extrapolate well to an estimated saturation value close to 3 μ_B, as expected for a system with three unpaired electrons per molecule.

A polycrystalline sample of **2** was used to measure the magnetic properties of the Fe(II) complex. The χT product was measured as a function of temperature from 300 to 1.81 K at an applied field of 10,000 Oe. At room temperature, the χT product is 3.00 cm^3 K mol^{-1} and upon cooling decreases, indicating the presence of dominant antiferromagnetic coupling interactions between the Fe(II) metal center and the DTDA radical. The value of χT drops to 2.1 cm^3 K mol^{-1} at 50 K and remains relatively constant upon further decrease in temperature, until 24 K where it begins to decrease again to a minimum of 1.15 cm^3 K mol^{-1} (Figure 6). This drop in χT below 24 K is presumably due to the onset of weak *inter*molecular antiferromagnetic interactions between complexes in the solid state, partial field saturation of the magnetization at 10,000 Oe, and a contribution from the magnetoanisotropy, which is apparent from the field-dependent magnetization measurements performed at various temperatures.

On the basis of the structure, complex **2** can be magnetically viewed as a spin dimer composed of an $S = 2$ *hs*-Fe(II) and an $S = {}^1/_2$ pyDTDA. The *intra*molecular exchange interaction can be modeled on the basis of an isotropic spin Heisenberg Hamiltonian:

$$\hat{H} = -2J\{\hat{S}_{Fe} \cdot \hat{S}_{Rad}\}$$

where J is the *hs*-Fe(II)−pyDTDA coupling constant and $\hat{S}_i$ is the spin operator ($S_{Fe} = 2$ and $S_{Rad} = {}^1/_2$). The theoretical expression for the magnetic susceptibility can be estimated by applying the van Vleck equation[13] in the weak field approximation:

$$\chi = \frac{N_A \mu_B^2 g_{av}^2}{4k_B T} \frac{10 + 35\exp(^{5J}/_{k_B T})}{2 + 3\exp(^{5J}/_{k_B T})}$$

where $g_{av} = g_{Fe} + g_{Rad}$. The experimental data were fitted down to 24 K with the following best fit parameters: $g_{av} = 2.11(2)$, $J/k_B = -60.3(3)$ K (see Figure 6). These indicate an $S_T = {}^3/_2$ spin ground-state for this system. Magnetization versus applied field (M vs H) was measured at 1.8, 3, 5, and 8 K. At the highest applied field (70,000 Oe), the magnetization is still increasing and the system does not appear to be close to approaching saturation (Inset, Figure 6). The highest measured magnetization value under these conditions is approximately 2 μ_B. This is still far from 3 μ_B, the value expected for a ground state $S_T = {}^3/_2$ system, and even further from the saturation value of 5 μ_B for a system with five unpaired electrons per molecule. This absence of magnetization saturation below 70,000 Oe is indicative of significant magnetoanisotropy, which is not uncommon for *hs*-Fe(II).[14]

The redox properties of compounds **1** and **2** were investigated as methylene chloride solutions at ambient temperature by cyclic voltammetry (CV). The voltammogram of **1** (Figure 7) is dominated by two redox processes from the neutral species: one oxidative (anodic peak potential $E_{pa} = 1.36$ V; cathodic peak potential $E_{pc} = 1.02$ V; peak-to-peak potential difference $\Delta E_{pp} = 340$ mV) and one reductive ($E_{pc} = -0.45$ V; $E_{pa} = -0.27$ V; $\Delta E_{pp} = 180$ mV). The relative peak area of the related anodic and cathodic peaks of both processes is affected by the sweep direction. CV analysis of the Ni(hfac)$_2$·2THF starting material under similar conditions shows that there are no redox processes observed within the solvent window. Like the plot of **1**, the CV of the uncoordinated pyDTDA ligand under similar conditions (see Supporting Information) reveals two redox processes from the neutral species: one oxidative ($E_{pa} = 0.91$ V; $E_{pc} = 0.75$ V; $\Delta E_{pp} = 160$ mV) and one reductive ($E_{pc} = -0.95$ V; $E_{pa} = -0.75$ V; $\Delta E_{pp} = 190$ mV). Thus, it is reasonable to suggest that all the redox processes observed

(13) van Vleck, J. H. *The Theory of Electric and Magnetic Susceptibility*; Oxford University Press: New York, 1932.

(14) (a) Oshio, H.; Hoshino, N.; Ito, T. *J. Am. Chem. Soc.* **2000**, *122*, 12602. (b) Manna, S. C.; Zangrando, E.; Ribas, J.; Chaudhuri, N. R. *Inorg. Chim. Acta* **2005**, *358*, 4497. (c) Kaneko, Y.; Kajiwara, T.; Yamane, H.; Yamashita, M. *Polyhedron* **2007**, *26*, 2074.

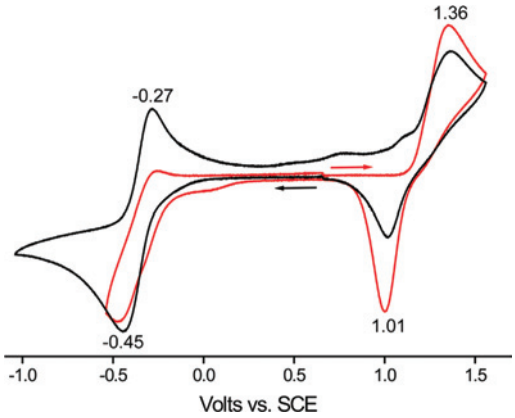

Figure 7. Cyclic voltammograms of **1** with an oxidative potential applied first (red) and with a reductive potential applied first (black). Performed in CH_2Cl_2: 2.26 mM analyte and 0.05 M nBu$_4$NPF$_6$ supporting electrolyte.

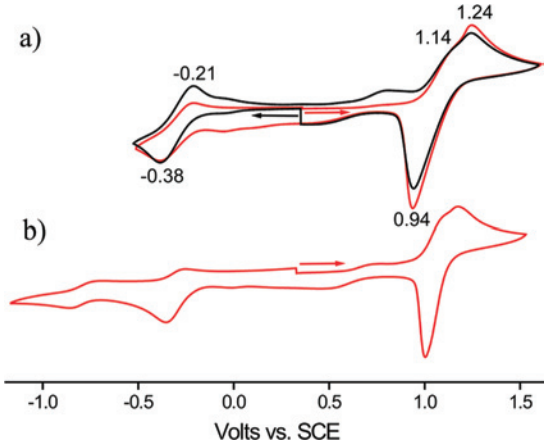

Figure 8. Cyclic voltammograms of **2** in CH_2Cl_2 with 0.05 M nBu$_4$NPF$_6$ supporting electrolyte. (a) Fresh solution (2.20 mM analyte) and sweep window restricted to major features only, with an oxidative potential applied first (red) and with a reductive potential applied first (black). (b) Full sweep, collected on an "old" solution (i.e., after multiple scans), showing all features within the solvent window.

for **1** are predominantly ligand based, albeit influenced by coordination to the metal.

In addition to the two dominant redox processes, there are also three other low peak area processes observed for **1**: a small peak at $E_{pc} = 0.03$ V when the oxidative direction is swept first and two small peaks at $E_{pa} = 0.76$ and 1.11 V when the reductive direction is swept first. Observations of this nature are typical for uncoordinated DTDA species in general,[15] and occur in the CV plots of the pyDTDA ligand itself (see Supporting Information); however, they are usually restricted to only one small anodic or one small cathodic peak, depending on scan direction. Similar small peak area processes have also been observed in the Co(II) and Mn(II) coordination complexes of pyDTDA.[16]

The cyclic voltammogram of **2** is more complex (Figure 8). Sweeping the applied potential in either the oxidative or reductive direction first gives rise to the same basic major features: two oxidative processes very close in potential at $E_{pa1} = 1.14$ V and $E_{pa2} = 1.24$ V with a related cathodic peak $E_{pc} = 0.94$ V ($\Delta E_{pp1} = 200$ mV; $\Delta E_{pp2} = 300$ mV), and one reductive process ($E_{pc} = -0.38$ V; $E_{pa} = -0.21$ V; $\Delta E_{pp} = 170$ mV). From the relative peak areas, it appears that the major processes at positive potential involve two consecutive one-electron oxidations and, upon reversal of the applied potential, re-reduction of both at effectively the same potential. The major reductive process at $E_{pc} = -0.38$ V appears to be a one electron process, based on relative peak areas. The relative peak areas of the cathodic and anodic peaks of this reductive process are affected by sweep direction.

We have measured the CV response of the pure, sublimed Fe(hfac)$_2$·2THF starting material under the same conditions (see Supporting Information) and observed two irreversible redox processes in the oxidative direction at $E_{pa1} = 1.48$ V and $E_{pa2} = 2.37$ V, the first of which is presumably associated with the Fe(II)/Fe(III) couple. No redox processes were observed in the reductive direction within the solvent window. It is worth noting that, to probe these processes accurately, it was necessary to use freshly sublimed material and freshly prepared solutions with a minimal number of scans. Scans including both an anodic and cathodic sweep gave rise to many more features; therefore, the oxidative processes and the reductive region were probed using two separate virgin solutions to determine which features were inherent to the Fe(hfac)$_2$·2THF and which arose from decomposition. It is also worth noting that, on the basis of the redox processes recorded for "Fe(hfac)$_2$",[17] these results may be highly solvent dependent.

Given the above observations, we can tentatively assign the redox processes of **2** as follows. The two oxidative processes at $E_{pa1} = 1.14$ V and $E_{pa2} = 1.24$ V may be the oxidation of the metal ion (Fe(II)/Fe(III)) and an independent ligand-based oxidation, although it is not possible to definitively assign which occurs at which potential. Upon reversal of the applied potential, re-reduction of both occurs effectively simultaneously, although broadness of the peak suggests two one-electron processes overlapping in potential as opposed to a two-electron process. The reductive process at $E_{pc} = -0.38$ V is presumably a ligand-based process, since no reductive processes are observed for (pure) Fe(hfac)$_2$·2THF within the solvent window.

In addition to the major features in the CV of **2**, there exist a number of smaller peak area features. When decreasing the applied potential through the 0.6 to 0 V region after sweeps including the major oxidative processes, numerous small features appear suggesting that some amount of decomposition occurs. When the major reductive process is interrogated applying a reductive potential first, a small oxidative feature at $E_{pa} = 0.8$ V appears. Again, this can be tentatively assigned as the result of a decomposition product since it does not appear in a virgin solution but persists in both oxidative and reductive scan directions once a solution has been electrochemically interrogated multiple times, as can be seen in Figure 8b. Finally, there is also a feature at more negative potential ($E_{pc} = -0.88$ V; $E_{pa} = -0.74$ V;

(15) Boeré, R. T.; Moock, K. H.; Parvez, M. *Z. Anorg. Allg. Chem.* **1994**, *620*, 1589.
(16) Britten, J.; Hearns, N. G. R.; Preuss, K. E.; Richardson, J. F.; Bin-Salamon, S. *Inorg. Chem.* **2007**, *46*, 3934.
(17) Villamena, F. A.; Horak, V.; Crist, D. R. *Inorg. Chim. Acta* **2003**, *342*, 125.

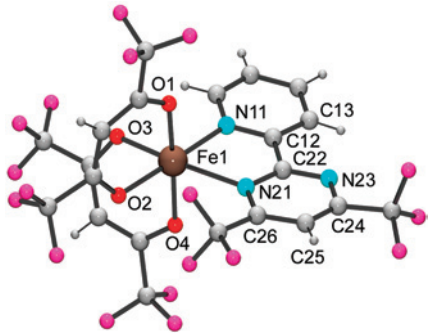

Figure 9. Crystal structure of decomposition product **3**.

ΔE_{pp} = 140 mV). The small relative peak area, and the observation that the relative peak area increases upon multiple scans, suggest that this is likely to be associated with a decomposition product as opposed to compound **2** itself. It should be noted that significant care was taken to ensure that measurements (Figure 8a) are reported on fresh solutions to determine which features are inherent to **2** and which arise as a result of decomposition.

The *hs*-Fe(II) complex **2** is unusually unstable compared to **1** and to other similar complexes.[6,16] Although **2** can be obtained as dark purple crystals by static vacuum sublimation, if care is not taken to ensure sufficient vacuum when sealing the apparatus, dark red crystals of the decomposition product **3** are recovered from the sublimation.

The single crystal X-ray structure of **3** reveals it to be a mononuclear Fe(II) complex with two hfac ligands and the previously unknown bidentate ligand 2-(2′-pyridyl)-4,6-bis(trifluoromethyl)pyrimidine **5** (Figure 9). The Fe(II) ion is in a pseudo-octahedral ligand environment. The bond lengths to the axially coordinated oxygen atoms of the hfac ligands, Fe1−O1 and Fe1−O4, are 2.038(3) and 2.070(3) Å, respectively. Those coordinated to the oxygen atoms in the equatorial plane, Fe1−O2 and Fe1−O3, are 2.063(3) and 2.097(4) Å, respectively. The iron ion is chelated by the novel ligand with bond lengths of 2.150(4) and 2.334(4) Å for Fe1−N11 and Fe1−N21, respectively. The two rings of this ligand are nearly coplanar, with a 6.9° angle of rotation between them.

Attempts to recrystallize **2** from dry, degassed solution under inert atmosphere resulted in the isolation of a second crystalline decomposition product **4** after a 6 month period. On the basis of the suspicion that the sample may have been inadvertently exposed to oxygen, **2** was heated into solution and allowed to sit for 5 days exposed to the air. The unit cell of the crystalline material recovered from this air-exposed solution matched that of product **4** from the original recrystallization attempt. The structure of **4** is an oxygen bridged iron tetramer with two hfac ligands on each of three iron atoms and two oxidized pyDTDA ligands chelated on the fourth (Figure 10). The crystal structure of this iron tetramer reveals a C_2 rotation along the Fe1−Fe3 axis such that there are only three unique iron positions (Fe2 and Fe2_2 are symmetry related positions) and the two oxidized pyDTDA ligands are symmetry related.

The iron oxide core is similar in structure to other known oxo-iron complexes with $\{Fe_4O_2\}^{8+}$ cores, including comparable bond lengths and angles.[18] In the known systems, all four iron atoms are reported to be in a +3 oxidation state. From the structure of **4** and by comparison with known structures, it is reasonable to assign the +3 oxidation state to all four iron atoms in this species as well. A list of selected bond lengths and angles is given in Table 2.

Complex **4** is structurally interesting for a number of reasons. It is the first example of a species in which multiple oxidized pyDTDA ligands are coordinated to a single metal ion and the first example of a metal cluster containing oxidized pyDTDA ligands. The manner in which the pyDTDA ligands have been oxidized is also novel. This type of 1,2,3,5-dithidiazolyl-1-oxide anion has never before been reported. Comparing this anion to the parent pyDTDA radical (when coordinated to Fe(II) in complex **2**), we find that the heterocyclic sulfur−sulfur bond distance is larger in the anion oxide (2.130(3) Å) than in the coordinated radical (2.077(7) Å). However, there is little difference between the sulfur−nitrogen bond distances S1−N8 in complex **2** (1.612(15) Å) and S2−N1 in complex **4** (1.624(5) Å). The sulfur−oxygen bond distance in **4** (1.544(5) Å) is significantly longer than a typical S=O double bond in a crystalline organic compound (e.g., C−SO_2−C fragment mean bond length is 1.436 Å)[19] but is slightly shorter than a typical S−O single bond (e.g., C−O−SO_2−C fragment mean bond length is 1.577 Å).[19]

Discussion

In our prior work with coordination complexes of the pyDTDA radical ligand, we have reported the structure and magnetic properties of Co(II), Mn(II) and Cu(II) complexes.[6,16] Herein we complete our series with the Ni(II) and Fe(II) complexes **1** and **2**.

The Ni(II) complex **1** and the Fe(II) complex **2** were prepared in a similar fashion to the previously reported Co(II),[6] Mn(II), and Cu(II) complexes of pyDTDA.[16] A solution of pyDTDA is reacted with an equimolar solution of the appropriate metal(hfac)$_2$·2THF. It is important that the solutions be dry since the pyDTDA radical decomposes upon exposure to moisture. Both the reagents and the resulting coordination complexes are soluble in organic media, so the solvent must be removed to recover the product. The crude coordination complexes can be purified for characterization purposes by bulk sublimation. Generally, a dynamic vacuum sublimation in a programmable three stage tube furnace equipped with a rotary vacuum pump provides adequate conditions to recover quantitative yields of metal coordination product; however, crystallography quality crystals are best generated under static vacuum sublimation. Typically, the metal coordination complexes show good thermal stability such that nearly quantitative yields can be recovered under sublimation conditions with no evidence of significant decomposition. The exception to this rule is the Fe(II) complex **2** which proved to be relatively

(18) Armstrong, W. H.; Roth, M. E.; Lippard, S. J. *J. Am. Chem. Soc.* **1987**, *109*, 6318.
(19) *CRC Handbook of Chemistry and Physics*, 72nd ed., Lide, D. R., Ed.; CRC Press: Boca Raton, 1991.

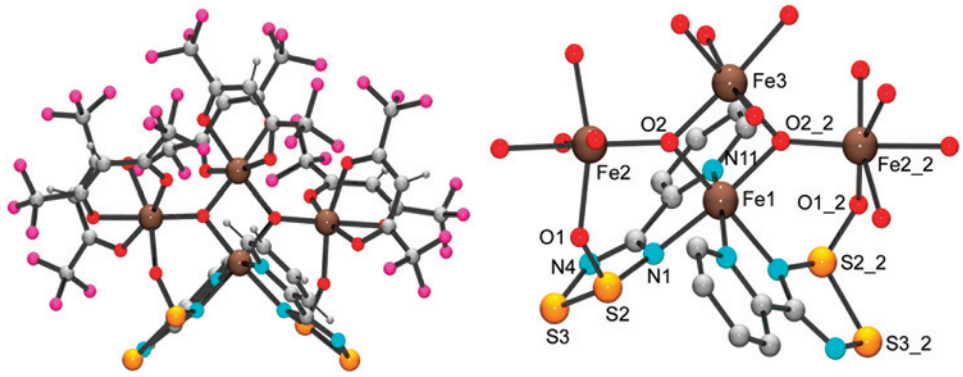

Figure 10. Crystal structure of decomposition product **4** (left) and of the iron, oxygen, and pyDTDA core of **4** with hydrogen atoms removed for clarity (right).

Table 2. Summary of Crystallographic Data for **4**, Including Select Bond Lengths and Bond Angles

molecular formula	$C_{42}H_{14}F_{36}Fe_4N_6O_{16}S_4$	cell angle β (deg)	101.365(6)
molecular weight(g/mol)	1894.23	cell formula units Z	4
space group	*C2/c*	temperature (K)	100(2)
cell lengths (Å): *a*, *b*, *c*	21.114(2), 17.348(2), 17.6397(14)		
distances (Å):			
Fe1−Fe3	2.863(2)	N1−Fe1	2.085(5)
Fe1−O2	1.953(4)	N11−Fe1	2.173(5)
Fe3−O2	1.946(4)	S2−O1	1.544(5)
Fe2−O2	1.877(4)	S2−S3	2.130(3)
Fe2−O1	2.031(5)	S2−N1	1.624(5)
angles (deg):			
Fe1−O2−Fe3	94.49(17)	Fe2−O1−S2	131.5(2)
Fe1−O2−Fe2	129.8(3)	N1−S2−S3	90.9(2)
Fe2−O2−Fe3	135.5(3)	N4−S3−S2	95.7(2)

thermally unstable and required a higher vacuum for sublimation. Under inadequate vacuum, decomposition product **3** was observed, reproducibly, in relatively high yields, to the exclusion of any other sublimed material. Exposure of a solution of Fe(II) complex **2** to air resulted in the formation of crystals of **4** over the period of a few days. This observation, too, is atypical of these coordination complexes. It should be noted that the Ni(II) complex **1**, although thermally stable, is nevertheless sensitive to air exposure. Although no visible change in the crystals of **1**, and no change in the elemental analysis, can be detected upon limited exposure to the air, ferromagnetic impurities are observed in the magnetometry measurements, and it is imperative that these samples be rigorously handled under inert atmosphere to obtain representative data.

Looking at the Mn(II) through Cu(II) series as a whole, it is interesting to note that the Mn(II) and Cu(II) complexes crystallize with the formation of π-dimers between neighboring pyDTDA ligands, but that the Co(II), Ni(II), and Fe(II) complexes are monomeric in the solid state and pack in isostructural, evenly spaced slipped π-stacks. This may be attributed to the coordination environment about the metal ion. In the Co(II), Ni(II), and Fe(II) species, the ligand sphere is pseudo-octahedral about the metal ion. In the Cu(II) species, an axial elongation typical for six-coordinate d^9 metal complexes is observed, and in the Mn(II) complex, the ligand sphere is closer to pseudo-trigonal. The distortions away from a pseudo-octahedral ligand distribution may shift the steric bulk of the hfac ligands enough to permit dimerization in the latter two species.

Looking at the trend in magnetic coupling properties, we find that Mn(II) and Fe(II) metal ions couple antiferromagnetically to the pyDTDA ligand and that Co(II), Ni(II) and Cu(II) couple ferromagnetically. If we use a pseudo-octahedral coordination sphere as a model, the trend in magnetic coupling correlates well to the number of unpaired electrons in σ-bonding versus π-bonding metal d orbitals. The greater the ratio in favor of unpaired electrons in σ-bonding orbitals, the more likely the magnetic coupling to the pyDTDA ligand, in which the unpaired electron is in a π-type molecular orbital, is to be ferromagnetic. This matches the magnetic coupling trend that can be predicted from a simple orbital overlap model.

The ferromagnetic coupling between the Ni(II) ion and the pyDTDA in complex **1** is quite strong ($J/k_B = +132$ K using the spin Hamiltonian definition $\boldsymbol{H} = -2J\{\boldsymbol{S}_{Ni}\cdot\boldsymbol{S}_{Rad}\}$). This is in keeping with other Ni(II) complexes of neutral radical ligands with comparable coordination geometries. For example, using the same spin Hamiltonian definition, the Ni(II)-radical coupling in $Ni(hfac)_2(IM2py)$ is reported to be $J/k_B = +137$ K (IM2py = 2-(2′-pyridyl-4,4,5,5-tetramethyl-4,5-dihydro-1*H*-imidazol-1-oxyl);[20] J/k_B is reported as +192 K for $[Ni(6bpyNO)_2]^{2+}$ (6bpyNO = 2,2′-bipyridin-6-yl *tert*-butyl nitroxide);[21] and for the $Ni(hfac)_2(pyvd)$ complex, $J/k_B = +173$ K (pyvd = 1,5-dimethyl-3-(2-pyridyl)-6-oxoverdazyl).[22]

(20) Tsukahara, Y.; Kamatani, T.; Iino, A.; Suzuki, T.; Kaizaki, S. *Inorg. Chem.* **2002**, *41*, 4363.
(21) Osanai, K.; Okazawa, A.; Nogami, T.; Ishida, T. *J. Am. Chem. Soc.* **2006**, *128*, 14008.

It is worth noting that in complex **2**, the Fe(II) ion is high spin. This is not surprising given that the hfac ligands are weak field ligands and that the analogous $Fe(hfac)_2(bipy)$ complex is also high spin.[23] From the magnetic data, we do not observe any temperature dependence of the spin of the Fe(II) ion; thus, no spin-crossover type behavior is observed.

Solution redox behavior can give insight into the electron distribution within the frontier molecular orbital manifold of the coordination complexes. First row transition metals typically have multiple accessible oxidation states and, as previously noted, we have performed cyclic voltammetric measurements of the $M(hfac)_2 \cdot 2THF$ starting materials to determine the redox activity of the $M(hfac)_2$ fragment (see Supporting Information). In addition, the pyDTDA ligand itself is redox active[6] and therefore has the potential to act as a non-innocent ligand. The pyDTDA ligand can be oxidized to a stable cation (which is also synthetically accessible)[6] and reduced to an anion (which has never been isolated). The CV responses of the coordination complexes are best viewed in light of those of the free pyDTDA ligand and the precursor $M(hfac)_2 \cdot 2THF$.

As previously noted, the CV of $Ni(hfac)_2 \cdot 2THF$ shows no redox features within the solvent window, so the CV of **1** is best compared to the CV of the pyDTDA ligand. In complex **1**, the pyDTDA ligand is acting as an electron donor toward the Ni(II) ion and can be expected to be electron deficient relative to the uncoordinated pyDTDA radical. This hypothesis is supported by the general shifting of both the oxidative and reductive redox processes of **1** to more positive potentials compared to those of the uncoordinated ligand. This implies that **1** is more readily reduced (difference in cathodic peak potential upon reduction $\Delta E_{pc} = 490$ mV) and less readily oxidized (difference in anodic peak potential upon oxidation $\Delta E_{pa} = 450$ mV) than the free pyDTDA.

Coordination of the pyDTDA to Ni(II) also has a significant effect on the peak potential difference of the oxidative process ($\Delta E_{pp/pyDTDA} = 160$ mV; $\Delta E_{pp/\mathbf{1}} = 340$ mV). This implies a dramatic rearrangement of electron density upon oxidation of **1** and suggests that the resulting cationic species is poorly represented as the $[pyDTDA]^+$ cation coordinated to the $Ni(hfac)_2$ fragment. It might be expected, for example, that a simple dissociation of a positively charged ligand (a poor electron donor) from the metal fragment could occur upon oxidation; however, there is no evidence suggesting that this is the case. The redox processes observed for **1** are completely reproducible over multiple scans with no increase in observed peak area of the small features and no appearance of new features associated with the free pyDTDA ligand.

There is little change in the peak potential difference of the reductive process ($\Delta E_{pp/pyDTDA} = 190$ mV; $\Delta E_{pp/\mathbf{1}} = 180$ mV) upon coordination; however, the relative peak areas of the anodic and cathodic components of this process are affected. This implies that any rearrangement of electron density that occurs upon reduction of **1** is comparable to that which occurs upon reduction of the uncoordinated pyDTDA ligand but that the reduced species $[\mathbf{1}]^-$ is less stable under these conditions than the $[pyDTDA]^-$ anion. It is, however, worth noting that reduction a DTDA radical in general results in a π^* HOMO and that, although observed in CV plots, no $[DTDA]^-$ anion has ever been isolated synthetically. In general, the CV features of **1** are very similar to those of the previously reported Co(II) coordination complex[16] suggesting similar electronic distributions in the frontier molecular orbital manifold of both complexes.

There are some general similarities between the solution redox behaviors of **1** and **2**. One dominant reductive process is observed at $E_{pc/\mathbf{1}} = -0.45$ V for **1** and at $E_{pc/\mathbf{2}} = -0.38$ V for **2**. Both have similar peak potential differences ($\Delta E_{pp/\mathbf{1}} = 180$ mV; $\Delta E_{pp/\mathbf{2}} = 170$ mV), not unlike that of the uncoordinated pyDTDA (vide supra), and both are shifted to less negative potentials compared to the free ligand, implying more facile reduction upon coordination. Given that $Fe(hfac)_2 \cdot 2THF$ is not reduced within the solvent window, the observed reductive process for **2**, like that of **1**, can tentatively be assigned as predominantly ligand-based.

Unlike complex **1**, two oxidative processes ($E_{pa1/\mathbf{2}} = 1.14$ V; $E_{pa2/\mathbf{2}} = 1.24$ V) occur in the CV of complex **2**. One of these is likely related to the oxidative process observed in **1**, and the other is likely a metal-centered process related to the Fe(II)/Fe(III) couple, given that $Fe(hfac)_2 \cdot 2THF$ is redox active at oxidative potentials under the applied conditions. Interestingly, these oxidative processes are at higher potentials than the oxidation of free pyDTDA ($E_{pa/pyDTDA} = 0.91$ V) and at lower potentials than the first oxidation of the $Fe(hfac)_2 \cdot 2THF$ starting material ($E_{pa1/Fe(hfac)2 \cdot 2THF} = 1.48$ V). This implies that electron donation from the pyDTDA ligand to the $Fe(hfac)_2$ fragment in complex **2** results in more facile oxidation of the metal and less facile oxidation of the ligand. The difference in peak potentials between the two anodic peaks and the common cathodic peak for these oxidative processes ($\Delta E_{pp1} = 200$ mV; $\Delta E_{pp2} = 300$ mV) implies a relatively extensive rearrangement of electron density upon oxidation of the complex, comparable to the observed oxidative behavior of **1**. In addition, complex **2** appears to be susceptible to decomposition since, unlike complex **1**, new features grow in peak area upon multiple scans. None of these, however, occur at potentials related to the redox processes of the starting materials, implying that simple dissociation of the pyDTDA ligand from the metal fragment is not a dominant decomposition pathway.

Complex **2** is unusually unstable compared to the other isolated metal complexes. During preliminary attempts to sublime **2** under insufficient vacuum, thermal decomposition reproducibly led to the recovery of crystalline **3**. This coordination complex includes the novel ligand **5**, 2-(2′-pyridyl)-4,6-bis(trifluoromethyl)pyrimidine. Ligand **5** appears to be the result of reaction between an hfac ligand and a pyDTDA ligand, involving the loss of two sulfur atoms and two oxygen atoms. Given that complex **3** also includes two intact hfac ligands, as does the parent complex **2**, it is reasonable to assume that the decomposition pathway

(22) Hicks, R. G.; Lemaire, M. T.; Thompson, L. K.; Barclay, T. M. *J. Am. Chem. Soc.* **2000**, *122*, 8077.
(23) Bailey, N. A.; Fenton, D. E.; Leal Gonzalez, M. S. *Inorg. Chim. Acta* **1984**, *88*, 125.

involves at least two molecules of **2**. No yellow crystalline material, typical of elemental sulfur, was observed in the sublimed material. The contents of the unsublimed ash from this decomposition were not examined. Possible co-products of this decomposition may include non-volatile iron oxides and/or iron sulfides.

Other metal analogues of compound **3** (i.e., Ni(II), Mn(II), Cu(II), or Co(II)) have never been observed from the sublimation of pyDTDA complexes analogous to **2**, regardless of the rigor with which the vacuum was monitored. This suggests that Fe(II) may somehow be involved in the decomposition pathway. To determine if ligand **5** can be formed via a reaction between pyDTDA and the hfac ligand in the absence of a transition metal under similar conditions, we have performed two experiments. For the first, we have reacted [Na(benzo-15-crown-5)][hfac] with a small excess of pyDTDA in dry CH_2Cl_2 at room temperature for 1 h. No precipitate was observed, so the solvent was removed in vacuo and the purple-black residue was sublimed at 100 °C. The purple-black crystals that formed to the exclusion of anything else were identified by IR spectroscopy as pure pyDTDA. The remaining unsublimed pale gray material appeared to be an admixture of colorless substance with a small amount of dark material. Analysis by IR and ^{1}H NMR spectroscopy identify this material as primarily unreacted [Na(benzo-15-crown-5)][hfac]. Thus, we conclude that pyDTDA does not react with the hfac ligand under similar conditions to the creation of **3** from **2**.

The second experiment was the reaction of pyDTDA with an equimolar amount of Hhfac in dry CH_2Cl_2. A color change was observed, indicating that a reaction had taken place, although it should be noted that this is not surprising since pyDTDA is likely to decompose in the presence of a protic acid. The brown residue that was obtained upon removal of the solvent was submitted to sublimation conditions; however, only elemental sulfur was recovered. Since **5** is very likely to be volatile and thermally stable, it is highly unlikely that this ligand was produced under similar conditions to the creation of **3** from **2**. Nevertheless, the non-volatile material was separated by column chromatography and analyzed by ^{1}H NMR. None of the resulting spectra were compatible with the structure of **5**.

An attempt to recrystallize **2** from dry, degassed chlorobenzene under inert atmosphere resulted in the recovery of the crystalline Fe(III) tetramer **4** after 6 months. The time frame of this decomposition was not closely monitored, and the atmosphere of the drybox in which the solution was stored had not been ideal throughout the period in question. Given the change in oxidation state of the iron, exposure to the air was hypothesized as the cause for the observed decomposition. To assess this possibility, **2** was heated into chlorobenzene in air and, and after 5 days, crystals of **4**, identified by single crystal X-ray, were observed. As noted in the discussion of the crystallographic structure of **4**, the $\{Fe_4O_2\}^{8+}$ core is known[18] but the oxidized pyDTDA ligand **6** is not. This is the first report of an oxide of a 1,2,3,5-dithiadiazolyl heterocycle. The structure of the 1,2,3,5-dithiadiazolyl-1-oxide anion **6** is, perhaps, most closely related to the known 1,2,3,5-oxathiadiazol-2-oxide heterocycle **7**.[24,25] Deprotonation of **7** and replacement of the ring oxygen atom with a sulfur atom yields the structure of **6**.

The mechanism of decomposition giving rise to **4** is unknown. The dark red crystals of **4** precipitated from solution as clean, shiny blocks. No other precipitates were observed and no co-products were identified.

Interestingly, reports of neutral radical coordination to Fe(II) are rare. For example, TEMPO forms stable adducts with $M(hfac)_2$ when M = Mn, Co, V=O, and Cu, but when TEMPO is reacted with $Fe(hfac)_2 \cdot 2H_2O$, two decomposition products are identified and no evidence is given of the adduct formation.[26] In this light, it is less surprising that **2** shows lower thermal stability than the other metal complexes in the series and perhaps more important that **2** can be prepared and purified without significant decompostion, given appropriate handling. Thus, **2** is a rare example of an Fe(II) coordination complex of a neutral paramagnetic ligand.

Conclusion

With the synthesis and characterization of Ni(II) complex **1** and a rare example of an Fe(II) complex of a neutral radical ligand **2**, we have completed a series of pyDTDA complexes of magnetic first row transition metal dications. We have shown that trends in the magnetic coupling can be predicted from a simple molecular orbital model and that trends in the formation of dimers in the solid state can be correlated to the coordination symmetry about the metal ion, also related to the d electron count.

We have discovered that the thermal stability of these complexes is generally good, with the exception of complex **2** for which a unique decomposition species **3**, containing the novel ligand **5**, has been identified. Attempts to generate **5** from reactions of pyDTDA with hfac under similar conditions have been unsuccessful, leading to speculation that **3** is the result of a relatively complex decomposition pathway involving more than one molecule of **2**.

Finally, we have identified an Fe(III) tetramer **4** that can be obtained reproducibly as a crystalline product of the air oxidation of **2** in solution. Interestingly, this material also contains a novel ligand **6** and, based on the structure, can also be assumed to form via a relatively complex pathway involving more than one molecule of **2**.

Acknowledgment. We thank Dr. A. Houmam at the University of Guelph for access to his electrochemical equipment. We thank Dr. J. Britten and C. Robertson at McMaster Analytical X-ray Diffraction Facility for data collection on **3**. K.E.P. thanks the Natural Science and Engineering Council (NSERC) of Canada for a Discovery Grant and the Government of Ontario for an Early Research Award. N.G.H.R. thanks the Government of Ontario for an Ontario Graduate Scholarship and NSERC for a postdoctoral fellowship (PDF). E.M.F. thanks NSERC for a CGS M

(24) Kohara, Y.; Kubo, K.; Imamiya, E.; Wada, T.; Inada, Y.; Naka, T. *J. Med. Chem.* **1996**, *39*, 5228.
(25) Charton, J.; Cousaert, N.; Bochu, C.; Willand, N.; Déprez, B.; Déprez-Poulain, R. *Tetrahedron Lett.* **2007**, *48*, 1479.

graduate scholarship. R.C. is grateful to the CNRS, the University of Bordeaux 1, and the Conseil Régional d'Aquitaine for financial support.

Supporting Information Available: Crystallographic information files (CIF) for **1** through **4**. Magnetization versus applied field at 100 K for **1** and **2**. CV plot of $Fe^{II}(hfac)_2 \cdot 2THF$ in CH_2Cl_2. Scan rate dependence plots for the CV plots of **1** and **2**. The CV plot of pyDTDA. This material is available free of charge via the Internet at http://pubs.acs.org.

IC800749B

(26) Ahlers, C.; Dickman, M. H. *Inorg. Chem.* **1998**, *37*, 6337.